PROCEEDINGS OF THE ROYAL SOCIETY A

rspa.royalsocietypublishing.org

Research

Article submitted to journal

Subject Areas:
Mechanics, Material Science, Structural Engineering

Keywords:
active materials, polymer gels, incremental analysis, stress-diffusion theory, prestressed state, swelling/shrinking.

Author for correspondence:
Marco Rossi
e-mail: marco.rossi@tu-dresden.de

Swelling and shrinking in prestressed polymer gels: an incremental stress-diffusion analysis

M. Rossi[1,2], P. Nardinocchi[3] and T. Wallmersperger[1,2]

[1] Institute of Solid Mechanics, TU Dresden, George-Bähr-Str. 3c, 01069 Dresden, Germany
[2] Dresden Center for Computational Materials Science (DCMS), TU Dresden, Hallwachsstraße 3, 01069 Dresden, Germany
[3] Department of Structural and Geotechnical Engineering, Sapienza Università di Roma, via Eudossiana 18, 00184 Roma, Italy

Polymer gels are porous fluid-saturated materials which can swell or shrink triggered by various stimuli. The swelling/shrinking induced deformation can generate large stresses which may lead to the failure of the material.
In the present research, a nonlinear stress-diffusion model is employed to investigate the stress and the deformation state arising in hydrated constrained polymer gels when subject to a varying chemical potential. Two different constraint configurations are taken into account: (i) elastic constraint along the thickness direction, and (ii) plane elastic constraint.
The first step entirely defines a compressed/tensed configuration. From there, an incremental chemo-mechanical analysis is presented. The derived model extends the classical linear poroelastic theory with respect to a prestressed configuration. Finally, the comparison between the analytical results obtained by the proposed model and a particular problem already discussed in literature for a stress-free gel membrane (one-dimensional test-case) will highlight the relevance of the derived model.

Royal Society Publishing
Informing the science of the future

© The Author(s) Published by the Royal Society. All rights reserved.

1. Introduction

Polymer gels are porous fluid-saturated elastic materials which swell and shrink in response to a large variety of environmental stimuli (e.g. temperature, light, pH, moisture). In the last decade, the scientific community [1–7] have been attracted by these promising materials due to their application in multifunctional devices.

The swelling/shrinking induced deformations, due to hydration and dehydration cycles, can generate large stresses which may significantly reduce performance, lead to failure, and determine fracture and fatigue phenomena [8] which in polymers have been rarely investigated within a modeling framework [9,10].

Two main approaches are widely employed in literature: nonlinear and linear formulations. As stated in Doi [11], the modeling of the key process in polymer gels, i.e. the swelling/shrinking process, is not a simple diffusion of a solvent through a polymer network. Rather, it is useful to consider the solvent-polymer mixture as a single homogenized continuum body which, once immersed in a solvent bath, swells until it reaches a homogeneous stress-free equilibrium (reference) state. Starting from that reference state a coupled chemo-mechanical problem is formulated within a nonlinear mechanics framework which allows to catch the huge swelling-induced deformations, defining the so called stress-diffusion theory [12–17]. However, in some situations, linear formulations can describe even moderately large deformations. Among these, the poroelastic model may be viewed as an incremental linear model based on small perturbations of a reference state which are induced by small changes in the environmental conditions [18–20]. Generally, linear stress-diffusion theories assume a stress-free reference configuration and there is no attempt to consider instead a prestressed one [11,12,20,21]. However, there are situations where it is useful to take into account the stressed state of a configuration, as for example in a single membrane of a fuel cell stack. In fact, hydration/dehydration cycles can induce the swelling/shrinking of each layer. Therefore, the single membrane can potentially be viewed as a gel body under mechanical loads or confinements, see also the work of Kusoglu et al. [22]. The effect of the surrounding bodies will be taken into account through linear springs which can generate a residual stress state into the gel. This aspect distinguishes the proposed model from the existing scientific literature and makes this manuscript an asset for future investigation.

The aim of this article is to develop an incremental approach of the stress-diffusion problem starting from a prestressed reference state, and to investigate eventual critical conditions which may be induced by mechanical confinements. We consider a gel body which lays in equilibrium and it is confined by a system of uniformly distributed elastic springs at rest in a bath of assigned chemical potential. The stiffness of the springs may be different between the in-plane and the out-of-plane direction. An increase (decrease) of the equilibrium chemical potential determines a water uptake (release), and, as a consequence, the gel swells (shrinks) while springs shorten (elongate) generating uniform compressive (tensile) stresses. Once this prestressed state is fully characterized, the incremental problem induced by a further small change in the chemical potential is formulated within a thermodynamically consistent framework. Finally, the incremental model is applied to investigate the incremental dynamics of a thin plate-like gel body, and estimates the space and time evolution of the key chemo-mechanical variables.

The paper is organized as follows. In Section 2, the well-known nonlinear stress-diffusion theory is recalled. In Section 3, the stress-diffusion model is applied to a gel with mechanical confinements. In Section 4, the thermodynamically consistent incremental problem is presented for a prestressed reference state. The proposed model is validated by showing that the standard poroelastic theory for a stress-free reference state and the incremental elastic theory from a prestressed state can be easily recovered. Finally, in Section 5, our model is applied to a plate-like body in order to obtain a one-dimensional time-dependent closed form solution.

2. Background

In this section, the well-known nonlinear stress-diffusion problem [14] is recalled in order to pave the way for the next investigation.

Three different states of a gel body are introduced: (i) a dry state $\mathcal{B}_d$, (ii) a swollen and stress-free state $\mathcal{B}_o$, and (iii) an actual state $\mathcal{B}_t$ (see figure 1). The model is based on two state variables: (i) the displacement field $\mathbf{u}_d(X_d, t)$ from $\mathcal{B}_d$ ($[\mathbf{u}_d] = \mathrm{m}$), and (ii) the molar water concentration per unit dry volume $c_d(X_d, t)$ ($[c_d] = \mathrm{mol\,m^{-3}}$). The point $X_d \in \mathcal{B}_d$ is a material point, $t \in \mathcal{T}$ is an instant of the time interval $\mathcal{T}$, and $x = X_d + \mathbf{u}_d(X_d, t)$ is the actual position of the point X_d at the time t.

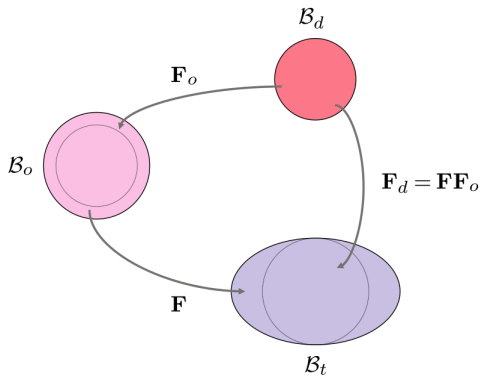

Figure 1. Dry gel state $\mathcal{B}_d$ (red shape) and the swollen stress-free state $\mathcal{B}_o$ (pink shape) only differ for a change in size, while the actual state $\mathcal{B}_t$ (violet shape) in general differs from $\mathcal{B}_d$ and $\mathcal{B}_o$ for a change in size and possibly in shape.

The thermodynamics of the model is derived from the classical Flory-Rehner model, which is based on a free energy ψ per unit dry volume ($[\psi] = \mathrm{J\,m^{-3}}$). The free energy ψ depends (i) on the deformation gradient $\mathbf{F}_d = \mathbf{I} + \nabla \mathbf{u}_d$ from the initial dry configuration of the polymer gel through an elastic component ψ_e, and (ii) on the molar solvent concentration c_d through a polymer-solvent mixing energy ψ_m. It holds: $\psi = \psi_e + \psi_m$. Moreover, it is assumed that a volumetric constraint, prescribing that changes in volume are only due to solvent absorption or release, holds:

$$\frac{dv_t}{dV_d} = \det \mathbf{F}_d = 1 + \Omega c_d \,, \tag{2.1}$$

being dV_d and dv_t two volume elements at $X_d \in \mathcal{B}_d$ and at $x \in \mathcal{B}_t$, respectively, and being Ω the molar volume of the solvent ($[\Omega] = \mathrm{m^3\,mol^{-1}}$).

The constitutive equation for the dry-reference stress $\mathbf{S}_d$ ($[\mathbf{S}_d] = \mathrm{Pa} = \mathrm{J\,m^{-3}}$) and for the chemical potential μ ($[\mu] = \mathrm{J\,mol^{-1}}$) stem from thermodynamic issues in the form

$$\mathbf{S}_d = \mathbf{S}_d(\mathbf{F}_d) - p\,\mathbf{F}_d^{\star} \quad \text{and} \quad \mu = \mu(c_d) + p\,\Omega \,, \tag{2.2}$$

with

$$\mathbf{S}_d(\mathbf{F}_d) = \frac{\partial \psi_e}{\partial \mathbf{F}_d} \quad \text{and} \quad \mu(c_d) = \frac{\partial \psi_m}{\partial c_d} \,, \tag{2.3}$$

where $\mathbf{F}^{\star} = (\det \mathbf{F})\mathbf{F}^{-T}$ and the pressure p ($[p] = \mathrm{Pa}$) is the reaction to the constraint (2.1). The Flory-Rehner thermodynamic model [23,24] prescribes a neo-Hookean elastic energy ψ_e and a polymer-solvent mixing energy:

$$\psi_e(\mathbf{F}_d) = \frac{G}{2}(\mathbf{F}_d \cdot \mathbf{F}_d - 3) \quad \text{and} \quad \psi_m(c_d) = \frac{RT}{\Omega}\, h(c_d) \,, \tag{2.4}$$

being G ($[G] = \mathrm{J\,m^{-3}}$) the shear modulus of the dry polymer. The variable $h(c_d)$ is given by:

$$h(c_d) = \Omega\, c_d \log \frac{\Omega\, c_d}{1 + \Omega\, c_d} + \chi \frac{\Omega\, c_d}{1 + \Omega\, c_d} \,, \tag{2.5}$$

being R ($[R] = \mathrm{J\,K^{-1}\,mol^{-1}}$), T ($[T] = \mathrm{K}$), and χ the universal gas constant, the temperature, and the dimensionless Flory parameter, respectively. From equations $(2.3)_1$ and $(2.4)_1$, we derive the constitutive equation for the dry-reference stress $\mathbf{S}_d(\mathbf{F}_d)$, while from equations $(2.3)_2$, $(2.4)_2$, and (2.5) we derive the constitutive equation for the chemical potential $\mu(c_d)$. It follows that

$$\mathbf{S}(\mathbf{F}_d) = G\mathbf{F}_d \quad \text{and} \quad \mu(c_d) = \frac{RT}{\Omega} h'(c_d)\,, \tag{2.6}$$

where the prime $(\,)'$ denotes the derivative with respect to the independent variable and

$$h'(c_d) = \Omega \left(\log \frac{\Omega\, c_d}{1+\Omega\, c_d} + \frac{1}{1+\Omega\, c_d} + \frac{\chi}{(1+\Omega\, c_d)^2} \right). \tag{2.7}$$

The balance equations of forces and solvent can be written starting from the balance of work and from the solvent mass conservation, respectively. In the reference state, it holds:

$$\mathtt{div}\,\mathbf{S}_d = \mathbf{0} \quad \text{and} \quad \dot{c}_d = -\mathtt{div}\,\mathbf{h}_d \quad \text{in} \quad \mathcal{B}_d\,, \tag{2.8}$$

with the referential solvent flux $\mathbf{h}_d$ constitutively determined in terms of a positive definite mobility tensor $\mathbf{M}_d = \hat{\mathbf{M}}(\mathbf{F}_d, c_d)$ as $\mathbf{h}_d = -\mathbf{M}_d \nabla\mu$ in such a way to satisfy the dissipation inequality. Boundary conditions have to be assigned to solve the coupled equations (2.8). As usual, we have: (i) Neumann-type boundary conditions on the stress vector $\mathbf{S}_d\mathbf{m}$ and on the solvent flux $\mathbf{h}_d \cdot \mathbf{m}$, or/and (ii) Dirichlet-type boundary conditions on the displacement $\mathbf{u}_d$ and on the concentration c_d:

$$\mathbf{S}_d\mathbf{m} = \mathbf{s} \quad \text{in} \quad \partial\mathcal{B}_{ds} \quad \text{and} \quad \mathbf{h}_d \cdot \mathbf{m} = q_d \quad \text{in} \quad \partial\mathcal{B}_{dq} \tag{2.9}$$

$$\mathbf{u} = \check{\mathbf{u}} \quad \text{in} \quad \partial\mathcal{B}_{du} \quad \text{and} \quad c_d = c_s \quad \text{in} \quad \partial\mathcal{B}_{dc} \tag{2.10}$$

with $\partial\mathcal{B}_{ds}$, $\partial\mathcal{B}_{dq}$, $\partial\mathcal{B}_{du}$, and $\partial\mathcal{B}_{dc}$ the portion of the dry boundary $\partial\mathcal{B}_d$ where tractions, fluxes, displacements, and concentration, respectively, are prescribed.

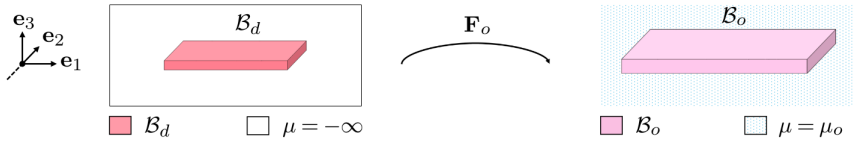

Figure 2. The free-swelling from $\mathcal{B}_d$ to $\mathcal{B}_o$ is determined by a change in the bath's chemical potential from the dry conditions $\mu = -\infty$ (white pattern) to $\mu = \mu_o$ (light blue pattern).

A distinguished problem is the free-swelling one. In that case, a free body is embedded into a solvent bath of chemical potential μ_o, boundary tractions are null and the confines are permeable. Moreover, the body is free and the boundary value c_s of the concentration on $\partial\mathcal{B}_d$ is assigned assuming that the gel is in equilibrium with the bath, that is,

$$\mu = \mu_o \quad \text{with} \quad \mu = \mu(c_s) + \Omega p\,, \quad \text{on} \quad \partial\mathcal{B}_d\,. \tag{2.11}$$

Looking for a homogeneous solution, mechanical and chemical balance laws prescribe $\mathbf{S}_d = \mathbf{0}$ and $\mu = \mu_o$. Denoting as $\mathbf{F}_o$ the gradient $\mathbf{F}_d$ of the deformation process from $\mathcal{B}_d$ to $\mathcal{B}_o$ (see figure 2), and according to the spherical form of $\mathbf{F}_o$, i.e. $\mathbf{F}_o = \lambda_o\mathbf{I}$, the mechanical balance yields the pressure p

$$G\mathbf{F}_o - p\,\mathbf{F}_o^\star = \mathbf{0} \quad \Rightarrow \quad p = \frac{G}{\lambda_o} = G_o\,, \tag{2.12}$$

being λ_o a uniform stretch. We denote G_o as the shear modulus reduced by the homogeneous free-swelling: $G_o = G/\lambda_o$. With this, the chemical balance yields a nonlinear equation relating μ_o

and λ_o

$$\mu(J_o) + G_o\,\Omega = \mu_o\,, \quad \text{with} \quad J_o = \lambda_o^3\,, \tag{2.13}$$

where, with a slight abuse of notation and exploiting the volumetric constraint (2.1), we set

$$h(c_d) = h(J_d) \quad \text{and} \quad h'(c_d) = \Omega\, h'(J_d)\,, \tag{2.14}$$

with

$$\mu(c_d) = \mu(J_d) = RT\Big(\log\frac{J_d - 1}{J_d} + \frac{1}{J_d} + \frac{\chi}{J_d^2}\Big)\,. \tag{2.15}$$

It may be useful to view the free-swollen state $\mathcal{B}_o$ as a reference configuration and to introduce the deformation gradient $\mathbf{F} = \mathbf{F}_d\,\mathbf{F}_o^{-1}$ from $\mathcal{B}_o$ to $\mathcal{B}_t$. Using the standard pull-back and push-forward approach, the swollen-reference stress $\mathbf{S}_o$ at $\mathcal{B}_o$ as well as the actual (Cauchy) stress $\mathbf{T}$ at $\mathcal{B}_t$ can be introduced as:

$$\mathbf{S}_o = \frac{1}{J_o}\mathbf{S}_d\mathbf{F}_o^T \quad \text{and} \quad \mathbf{T} = \frac{1}{J_d}\mathbf{S}_d\mathbf{F}_d^T\,. \tag{2.16}$$

Using equations $(2.2)_1$, $(2.3)_1$, $(2.4)_1$, we obtain the following relations:

$$\mathbf{S}_o = \frac{G}{J_o}\mathbf{F}\mathbf{F}_o\mathbf{F}_o^T - p\mathbf{F}^\star \quad \text{and} \quad \mathbf{T} = \frac{1}{J_d}\,G\,\mathbf{F}_d\,\mathbf{F}_d^T - p\mathbf{I}\,. \tag{2.17}$$

3. Tension and compression states

In this section, the general stress-diffusion model, given in Section 2, is employed to investigate the hydration/dehydration of a gel with boundary springs. The final state $\mathcal{B}_t = \mathcal{B}$ is not stress-free and it is assumed as new prestressed reference configuration for the next step, given in Section 4. We consider a plate-like body is in free state $\mathcal{B}_o$ into a bath of chemical potential μ_o, (see figure 2). The end faces $\mathcal{P}^\pm$ of the body have a unit normal $\pm\mathbf{e}_3$, the in-plane sizes have a length L_o and the thickness of the body is h_o. Moreover, we denote as $\mathbf{m}$ the unit normal at the mantle (lateral boundary) $\mathcal{M}$ of the body. Therefore, $\partial\mathcal{B}_o \equiv \{\mathcal{P}^+ \cup \mathcal{P}^- \cup \mathcal{M}\}$. We assume that the body is anchored all over the permeable boundary through a uniform field of linear elastic springs mimicking the effect of surrounding bodies. We assume that the springs are relaxed at $\mathcal{B}_o$, and that their stiffness may be different between the in-plane k and the transverse direction $k_\perp$ (with $[k, k_\perp] = \mathrm{Pa}$) (see figure 3).

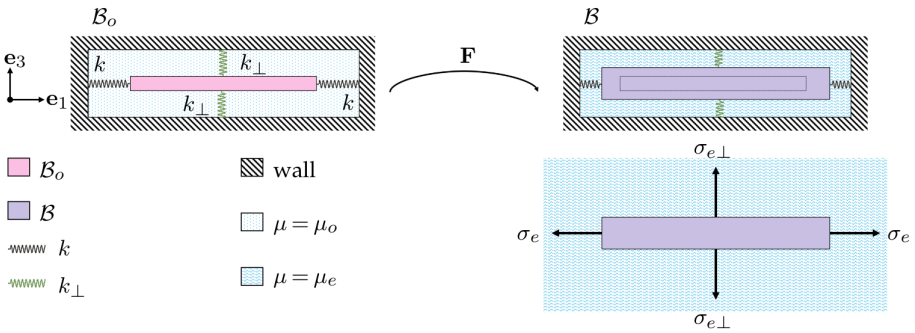

Figure 3. Change of the bath's chemical potential from μ_o (light blue pattern) to μ_e (blue pattern) determines the deformation $\mathbf{F}$ and the tractions σ_e and $\sigma_{e\perp}$ on the boundary $\partial\mathcal{B}$.

A change in the chemical potential of the bath, from μ_o to μ_e, determines a new process from $\mathcal{B}_o$ to $\mathcal{B}$, whose deformation gradient is denoted as $\mathbf{F}$. The latter deformation process is influenced (i) by the stiffnesses k and $k_\perp$ of the boundary springs acting on the mantle and on the end faces, respectively, and (ii) by the chemical potential μ_e. We assume that $\mathbf{F}$ has a transversely isotropic structure which is described by the homogeneous stretches λ and $\lambda_\perp$: $\mathbf{F} = \lambda\hat{\mathbf{I}} + \lambda_\perp\mathbf{e}_3 \otimes \mathbf{e}_3$, where

we set $\lambda_1 = \lambda_2 = \lambda$, $\lambda_3 = \lambda_\perp$, and $\hat{\mathbf{I}} = \mathbf{I} - \mathbf{e}_3 \otimes \mathbf{e}_3$. Mechanical and chemical boundary conditions prescribe that

$$\mathbf{T}\mathbf{m} = \sigma_e \mathbf{m} \quad \text{on} \quad \mathcal{M} \quad \text{and} \quad \mathbf{T}\mathbf{e}_3 = \sigma_{e\perp}\mathbf{e}_3 \quad \text{on} \quad \mathcal{P}^{\pm}\,, \tag{3.1}$$

whereas $\mu = \mu_e$ all over $\partial\mathcal{B}$. Assuming that the homogeneous (Cauchy) stress shares the transversely isotropic structure of $\mathbf{F}$ and has the form $\mathbf{T} = \sigma\hat{\mathbf{I}} + \sigma_\perp \mathbf{e}_3 \otimes \mathbf{e}_3$, we have

$$\sigma = \sigma_e\,, \quad \sigma_\perp = \sigma_{e\perp} \quad \text{and} \quad \mu = \mu_e\,, \tag{3.2}$$

everywhere in $\mathcal{B}$. We assume that the following representation holds for the external tractions σ_e and $\sigma_{e\perp}$ due to the boundary springs:

$$\sigma_e = -k\,(\lambda - 1) \quad \text{and} \quad \sigma_{e\perp} = -k_\perp\,(\lambda_\perp - 1)\,. \tag{3.3}$$

The new equilibrium state is characterized by the external chemical potential μ_e. The corresponding equation of chemical equilibrium prescribes that:

$$\mu(JJ_o) + \Omega p = \mu_e \quad \text{with} \quad J = \lambda^2\lambda_\perp\,. \tag{3.4}$$

When the chemical potential varies, the swelling-induced deformation of the body determines a change in the length of springs while uniform normal stresses act on $\partial\mathcal{B}$. We consider the following scenarios.

- The chemical potential decreases, that is $\mu_e < \mu_o$: the gel expels solvent and shrinks ($\lambda < 1$ and $\lambda_\perp < 1$), so reducing its volume, the springs elongate, thus generating uniform tensile stresses σ_e and $\sigma_{e\perp}$ (tension zone).
- The chemical potential increases, that is $\mu_e > \mu_o$: the gel absorbs solvent and swells ($\lambda > 1$ and $\lambda_\perp > 1$), so increasing its volume as shown in figure 3, the springs shorten, thus generating uniform compressive stresses σ_e and $\sigma_{e\perp}$ (compression zone).

When $\mu_e = \mu_o$, the springs stay relaxed and no further deformation processes take place ($\mathbf{F} = \mathbf{I}$). In the general case, equations (3.2) define the homogeneous problem to be solved to characterize the state $\mathcal{B}$. The constitutive equations $(2.17)_2$ and (3.4), for both the stress and the chemical potential, are given by

$$\sigma = \frac{G_o}{\lambda_\perp} - p\,, \quad \sigma_\perp = \frac{G_o\lambda_\perp}{\lambda} - p \quad \text{and} \quad \mu = \mu(JJ_o) + \Omega p\,. \tag{3.5}$$

By inserting equations (3.2) into equations (3.5) the following nonlinear system with three unknowns $(\lambda\,, \lambda_\perp\,, p)$ is defined:

$$\begin{aligned} &\frac{G_o}{\lambda_\perp} - p = -k\,(\lambda - 1)\,, \\ &\frac{G_o\lambda_\perp}{\lambda^2} - p = -k_\perp\,(\lambda_\perp - 1)\,, \\ &RT\left(\log\frac{JJ_o - 1}{JJ_o} + \frac{1}{JJ_o} + \frac{\chi}{J^2J_o^2}\right) + \Omega p = \mu_e\,. \end{aligned} \tag{3.6}$$

We studied the two limit cases: (i) $k = 0$ and (ii) $k_\perp = 0$, corresponding to a body $\mathcal{B}$ elastically constrained only at the end faces $\mathcal{P}^{\pm}$ or at the mantle $\mathcal{M}$, respectively. The solutions of the two problems are investigated and represented in figures 4 and 5, by considering $\mu_o = -50\ \mathrm{J\,mol^{-1}}$ and $G = 10 \times 10^4$ Pa [16] (to which corresponds $\lambda_o = 1.615$ and $G_o = 6.193 \times 10^4$ Pa). A recap of the employed constants and parameters is presented in Table 1.

Table 1. Constants and parameters employed in the proposed simulations [16].

Parameter	Value	Unit
R	8.3145	$\mathrm{J\,mol^{-1}\,K^{-1}}$
T	288.65	K
Ω	6×10^{-5}	$\mathrm{m^3\,mol^{-1}}$
G	10×10^{4}	Pa
χ	0.2	–
λ_o	1.615	–
μ_o	-50	$\mathrm{J\,mol^{-1}}$

(i) Elastic constraints along the thickness ($k = 0$)

In the first case, elastic constraints are present only in the thickness direction, that is the body $\mathcal{B}_o$ is constrained only at the end faces $\mathcal{P}^{\pm}$, while the stiffness of the springs on the mantle $\mathcal{M}$ is set to zero, i.e. $k = 0$. The system (3.6) reduces to the following equations with unknowns λ and $\lambda_\perp$:

$$\frac{\lambda_\perp}{\lambda_o \lambda^2} - \frac{1}{\lambda_o \lambda_\perp} = -\alpha_\perp \left(\lambda_\perp - 1\right), \quad \mu(J J_o) + \Omega \frac{G_o}{\lambda_\perp} = \mu_e \,, \tag{3.7}$$

where we set $\alpha_\perp = k_\perp / G$. Once, solved them, the pressure p can be determined from the equation $(3.6)_1$ or $(3.6)_2$. An overview of the solution of the problem can be obtained by looking at the intersection points in the λ–$\lambda_\perp$ plane of the equations (3.7), see figure 4(A). Moreover, figure 4(B) shows the stress state corresponding to a choice of μ_e and $\alpha_\perp$.

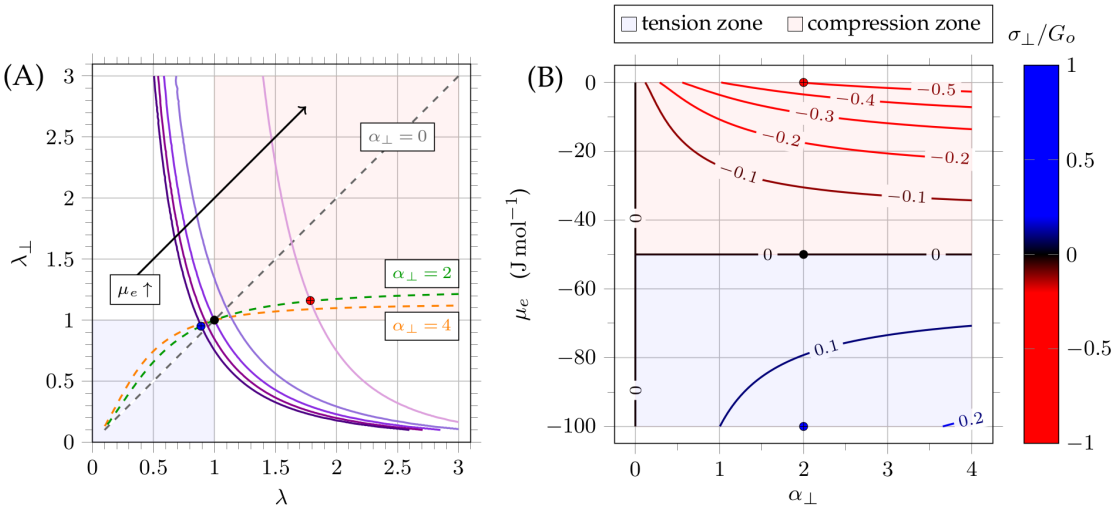

Figure 4. (A) The iso-potential lines $\mu_e = -100, -75, -50, -25, 0$ J mol^{-1} range from $\mu_e = -100$ J mol^{-1} (dark violet solid line) to $\mu_e = 0$ J mol^{-1} (light violet solid line) and are obtained from equation $(3.7)_2$. Dashed lines are obtained from equation $(3.7)_1$ for $\alpha_\perp = 0, 2, 4$ (gray, green, and orange dashed lines, respectively). The intersections between dashed and solid lines deliver the $\lambda, \lambda_\perp$ solutions corresponding to those specific values of μ_e and $\alpha_\perp$. (B) Isolines of the dimensionless stress $\sigma_\perp / G_o$. The red, black, and blue crossed dots correspond to the same states.

The solid isolines in figure 4(A) show the chemical potential in equation $(3.7)_2$ corresponding to $\mu_e = -100, -75, -50, -25, 0$ J mol^{-1}, according to the arrow's direction (solid lines with different shades of violet). The dashed isolines correspond to equation $(3.7)_1$ for $\alpha_\perp = 0, 2, 4$ (gray, green and orange dashed line, respectively). All the possible solutions of the system (3.7) are given by the intersections between the solid and the dashed lines. As it is expected, for $\mu_e = \mu_o = -50$

$\mathrm{J\,mol^{-1}}$ (intermediate violet solid line) and for each value of $\alpha_\perp$, the solution is trivial: no further deformation from $\mathcal{B}_o$ is induced, $\lambda = \lambda_\perp = 1$ and $\mathbf{F} = \mathbf{I}$ (black dot). For values $\mu_e > -50$ $\mathrm{J\,mol^{-1}}$ (lighter violet solid lines), all the solutions show $\lambda > 1$ and $\lambda_\perp > 1$, that is the gel absorbs solvent, swells and undergoes compression while the springs shorten (light red area). In absence of springs, that is for $\alpha_\perp = 0$ (gray dashed line), the body increases its volume in stress-free conditions without any changes in shape ($\lambda = \lambda_\perp$). However, for values $\alpha_\perp \neq 0$ and increasing from $\alpha_\perp = 2$ (green dashed lines) to $\alpha_\perp = 4$ (orange dashed lines), fixed $\mu_e = 0$ $\mathrm{J\,mol^{-1}}$ (light violet solid line), the plane stretch λ increases while the transverse stretch $\lambda_\perp$ decreases, being the latter (out-of-plane) direction constrained by stiffer springs ($k_\perp > k$). For values $\mu_e < -50$ $\mathrm{J\,mol^{-1}}$ (darker violet solid lines), the opposite behavior is observed. All the solutions show for $\lambda < 1$ and $\lambda_\perp < 1$, that the gel expels solvent, shrinks and undergoes tension while the springs elongate (light blue area). The solid isolines in figure 4(B) show the dimensionless stress $\sigma_\perp/G_o$. The light red and the light blue colored parts of the panel identify the same compression and tension zones as in figure 4(A). The black isolines identify the zero stress states corresponding to $\mu_e = \mu_o$, for any values of $\alpha_\perp$ (horizontal black line), and to $\alpha_\perp = 0$, for any values of μ_e (vertical black line). Large stresses are achieved for large chemical stimulus $|\mu_e - \mu_o| \gg 0$ and for stiffer springs, i.e. for $\alpha_\perp$ increasing from 0 to 4.

(ii) Plane elastic constraints ($k_\perp = 0$)

In the second case, elastic constraints are present only in the in-plane direction, that means that the body $\mathcal{B}_o$ is constrained at the mantle $\mathcal{M}$, while the stiffness of the springs on the end faces $\mathcal{P}^\pm$ is zero, i.e. $k_\perp = 0$. The system (3.6) reduces to the following equations:

$$\frac{1}{\lambda_\perp \lambda_o} - \frac{\lambda_\perp}{\lambda_o \lambda^2} = -\alpha\,(\lambda - 1)\,, \quad \mu(J J_o) + \Omega \frac{G_o \lambda_\perp}{\lambda^2} = \mu_e\,, \tag{3.8}$$

in the unknowns λ and $\lambda_\perp$ and with $\alpha = k/G$. As in the previous case, figures 5(A) and 5(B) show the solution of the problem through the same graphical representation in the λ–$\lambda_\perp$ plane, together with a representation of the stress state corresponding to a choice of μ_e and α.

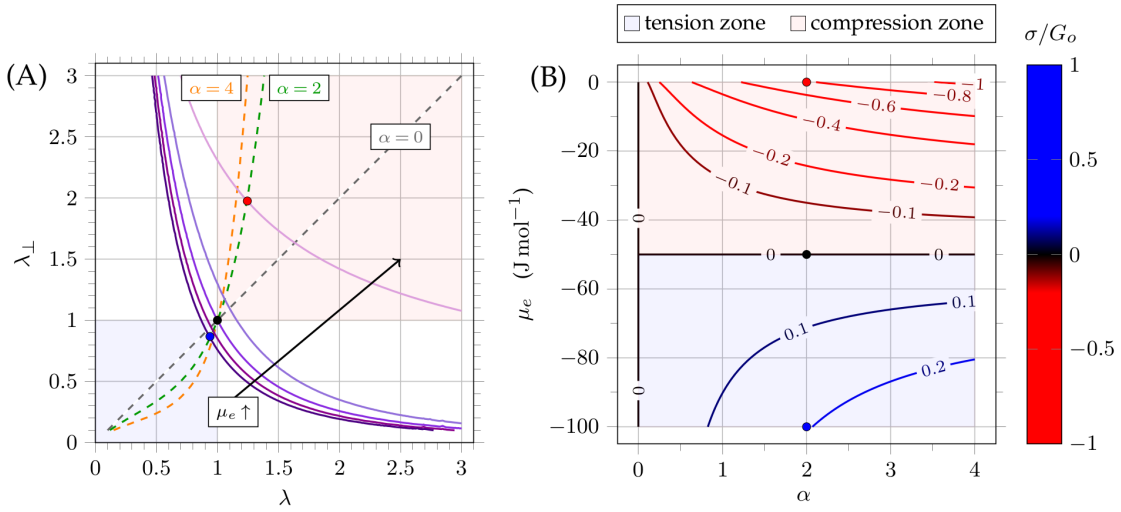

Figure 5. (A) The iso-potential lines $\mu_e = -100, -75, -50, -25, 0$ $\mathrm{J\,mol^{-1}}$ range from $\mu_e = -100$ $\mathrm{J\,mol^{-1}}$ (dark violet solid line) to $\mu_e = 0$ $\mathrm{J\,mol^{-1}}$ (light violet solid line) and are obtained from equation $(3.8)_2$. Dashed lines are obtained from equation $(3.8)_1$ for $\alpha = 0, 2, 4$ (gray, green, and orange dashed lines, respectively). The intersections between dashed and solid lines deliver the $\lambda, \lambda_\perp$ solutions corresponding to those specific values of μ_e and α. (B) Isolines of the dimensionless stress σ/G_o. The red, black, and blue dots correspond to the same states.

All possible solutions of the system (3.8) are given by the intersections between the solid and the dashed lines in figure 5(A). The bisector of the λ–$\lambda_\perp$ plane (gray dashed line) represents the solution of the equation $(3.8)_1$ corresponding to $\alpha = 0$. The trivial solution is identified by the intersection of each curve of α (gray, orange, and orange dashed lines) with the solution of the equation $(3.8)_2$ corresponding to $\mu_e = \mu_o = -50\ \mathrm{J\,mol^{-1}}$ (black dot). Compression and tension zones are obtained for values $\mu_e > -50\ \mathrm{J\,mol^{-1}}$ (lighter violet solid line) and $\mu_e < -50\ \mathrm{J\,mol^{-1}}$ (darker violet) solid line, respectively. The intersections of the isoline $\mu_e = 0\ \mathrm{J\,mol^{-1}}$ (light violet solid line) with the isolines going from $\alpha = 2$ (green dashed line) to $\alpha = 4$ (orange dashed line), identify an opposite situation with respect to the previous problem with plane elastic constraints: transverse stretches $\lambda_\perp$ increase while plane stretches λ decrease, being the in-plane direction constrained by stiffer springs ($k > k_\perp$). The solid lines in figure 5(B) are the contour plots of the dimensionless stress σ/G_o. As expected, larger stresses are obtained with respect to the case with elastic constraints along the thickness, see figure 4(B), due to the presence of an higher number of springs. In fact, plane elastic constraints are placed in two directions: $\mathbf{e}_1$ and $\mathbf{e}_2$. The red (compression), black (stress-free), and blue (tension) crossed dots identify the same states in both figures. It is worth noting that an appropriate combination of the two parameters (α and μ_e) results in a particular stress state (compression or tension) within the gel sheet.

4. Incremental analysis of the stress-diffusion problem

In this section, once the state $\mathcal{B}$ is entirely characterized according to the formulation given in Section 3, we want to investigate a further hydration/dehydration of the gel under the assumption of small changes. We present a thermodynamically consistent incremental analysis of the stress-diffusion problem from the prestressed reference configuration $\mathcal{B}$.

When a further change in the chemical potential μ_e is introduced, a new deformation process from $\mathcal{B}$ is determined, whose gradient is denoted as $\tilde{\mathbf{F}}$. Therefore, the gradient of the deformation process from $\mathcal{B}_d$ to $\mathcal{B}_t$ can be represented in terms of a sequence of deformation processes from $\mathcal{B}_d$ as $\mathbf{F}_d = \tilde{\mathbf{F}}(\mathbf{F}\mathbf{F}_o)$ (see figure 6).

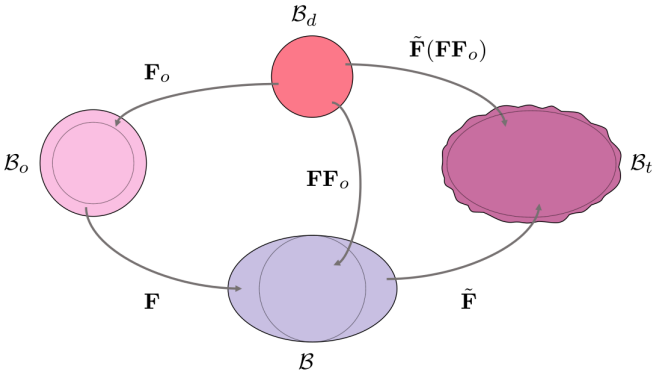

Figure 6. Sequence of deformation processes from the dry state $\mathcal{B}_d$ (red shape) to the actual state $\mathcal{B}_t$ (purple shape).

For a chemical potential changing from μ_e to $\mu_e + \epsilon\tilde{\mu}$, with $\epsilon \ll 1$, we state that the change is small and the whole induced mechanical problem can be studied through an incremental approach, based on a linearized analysis around the stressed state $\mathcal{B}$. Therefore, $\tilde{\mathbf{F}} = \tilde{\mathbf{F}}(\epsilon) = \mathbf{I} + \epsilon\mathbf{H}$, that is, $\tilde{\mathbf{F}}$ is a small deformation superimposed to the deformation $\mathbf{F}\mathbf{F}_o$ and $\tilde{\mathbf{F}}(0) = \mathbf{I}$ [21].

Correspondingly, the reference stress $\mathbf{S}$ is represented as $\mathbf{S}(\epsilon) = \mathbf{S}_0 + \epsilon\tilde{\mathbf{S}}$, with $\mathbf{S}_0$ as the stress at $\mathcal{B}$ (corresponding to $\tilde{\mathbf{F}} = \mathbf{I}$) and with $\tilde{\mathbf{S}}$ the so called incremental stress. It is worth noting that $\mathbf{S}_0$ is equal to the Cauchy stress $\mathbf{T}_0$ at $\mathcal{B}$, corresponding to the deformation process $\mathbf{F}_d = \mathbf{F}\mathbf{F}_o$, usually called *prestress*, and

$$\mathbf{S}_0 = \mathbf{T}_0 = \frac{1}{J\,J_o}\,G\,(\mathbf{F}\mathbf{F}_o)\,(\mathbf{F}\mathbf{F}_o)^T - p_0\mathbf{I}\ , \tag{4.1}$$

being $p(\epsilon) = p_0 + \epsilon\tilde{p}$, with p_0 the pore pressure at $\mathcal{B}$ corresponding to $\tilde{\mathbf{F}} = \mathbf{I}$. [1] The latter variable, i.e. p, is given by the solution of equations (3.6). Moreover, the form of the prestress $\mathbf{S}_0$ depends on the boundary elastic springs which also determines the deformation map $\mathbf{F}$.
We also assume that the concentration c per unit of reference volume $\mathcal{B}$ and the chemical potential μ within the body, both existing at $\mathcal{B}_t$, allow a similar representation:

$$c = c_0 + \epsilon\gamma \quad \text{and} \quad \mu = \mu_e + \epsilon\tilde{\mu}\,, \tag{4.2}$$

where c_0 and γ are the concentration at $\mathcal{B}$ and its increment, respectively, both per unit volume in $\mathcal{B}$, and μ_e is the value of the chemical potential at $\mathcal{B}$ with $\tilde{\mu}$ its increment.
Finally, we deal with the incompressibility constraint: starting from the equation (2.1) and by using the proper change of density, we get [2]

$$\frac{dv_t}{dV_d} = \tilde{J}JJ_o = 1 + \Omega c_d = 1 + \Omega JJ_o c \quad \Rightarrow \quad \tilde{J} = \frac{1}{JJ_o} + \Omega c = 1 + \Omega(c - c_0) = 1 + \Omega\epsilon\gamma\,. \tag{4.3}$$

Moreover, being $\tilde{J} = \det\tilde{\mathbf{F}}$, we also get

$$\tilde{J}(\epsilon) = 1 + \epsilon\mathbf{I}\cdot\mathbf{H} = 1 + \Omega\epsilon\gamma\,. \tag{4.4}$$

Therefore, the incremental version of the incompressibility constraint prescribes that $\Omega\gamma = \mathbf{I}\cdot\mathbf{H}$.

(a) Incremental thermodynamics

Following Ref. [21], we analyze the incremental problem starting from a $O(\epsilon^2)$ thermodynamics, that is, we develop both the external work and the time rate of the free energy up to $O(\epsilon^2)$.
The mechanical and the chemical external work $\mathcal{W}(\mathcal{P})$, being $\mathcal{P} \subset \mathcal{B}$, can be expressed as

$$\mathcal{W}(\mathcal{P}) = \int_{\mathcal{P}} \left(\mathbf{S}\cdot\dot{\tilde{\mathbf{F}}} + \mu\dot{c} - \mathbf{h}\cdot\nabla\mu\right)\,, \tag{4.5}$$

with $\mathbf{h} = \epsilon\tilde{\mathbf{h}}$. Implementing the incremental approximations and deriving the time rate of the concentration field from the volumetric constraint $\det\tilde{\mathbf{F}} = \tilde{J} = 1 + \Omega(c - c_0)$ as

$$\dot{c} = \frac{1}{\Omega}\left[\mathbf{I} + \epsilon(\mathbf{I}\cdot\mathbf{H})\mathbf{I} - \epsilon\mathbf{H}^T\right]\cdot\epsilon\dot{\mathbf{H}}\,, \tag{4.6}$$

we get for the internal work density w the following representation

$$\begin{aligned} w = {} & \epsilon\left(\mathbf{S}_0\cdot\dot{\mathbf{H}} + \frac{\mu_e}{\Omega}(\mathbf{I}\cdot\dot{\mathbf{H}})\right) \\ & + \epsilon^2\left(\tilde{\mathbf{S}}\cdot\dot{\mathbf{H}} + \frac{\mu_e}{\Omega}\left((\mathbf{I}\cdot\mathbf{H})\mathbf{I}\cdot\dot{\mathbf{H}} - (\mathbf{H}^T\cdot\dot{\mathbf{H}})\right) + \frac{\tilde{\mu}}{\Omega}(\mathbf{I}\cdot\dot{\mathbf{H}}) - \tilde{\mathbf{h}}\cdot\nabla\tilde{\mu}\right)\,. \end{aligned} \tag{4.7}$$

The free energy density per unit volume of $\mathcal{B}$ is defined from ψ through a change in density as

$$\frac{1}{JJ_o}(\psi_e(\mathbf{F}_d) + \psi_m(c_d)) \quad \text{with} \quad \mathbf{F}_d = \tilde{\mathbf{F}}\mathbf{F}\mathbf{F}_o \quad \text{and} \quad \psi_m(c_d) = \frac{RT}{\Omega}h(\det(\tilde{\mathbf{F}}\mathbf{F}\mathbf{F}_o))\,, \tag{4.8}$$

being $\tilde{J}JJ_o = \det(\tilde{\mathbf{F}}\mathbf{F}\mathbf{F}_o) = \det\mathbf{F}_d$ and $\tilde{J} = \tilde{J}(\epsilon)$. We get

$$\frac{1}{JJ_o}\psi_e(\tilde{\mathbf{F}}(\epsilon)\mathbf{F}\mathbf{F}_o) = \frac{3}{2}G + \epsilon G\mathbf{H}\mathbf{F}\mathbf{F}_o\cdot\mathbf{F}\mathbf{F}_o + \frac{1}{2}\epsilon^2 G\mathbf{H}\mathbf{F}\mathbf{F}_o\cdot\mathbf{H}\mathbf{F}\mathbf{F}_o\,, \tag{4.9}$$

and

$$\begin{aligned} \frac{1}{JJ_o}h(\tilde{J}(\epsilon)JJ_o) = {} & \frac{1}{JJ_o}h(JJ_o) + \epsilon h'(JJ_o)(\mathbf{I}\cdot\mathbf{H}) + \\ & \frac{1}{2}\epsilon^2\left(JJ_o h''(JJ_o)(\mathbf{I}\cdot\mathbf{H})^2 + h'(JJ_o)\left((\mathbf{I}\cdot\mathbf{H})\mathbf{I} - \mathbf{H}^T\right)\cdot\mathbf{H}\right)\,, \end{aligned} \tag{4.10}$$

[1] Equation (4.1) is obtained by using equation $(2.17)_2$ for the deformation process $\mathbf{F}_d = \mathbf{F}\mathbf{F}_o$.
[2] The identity $1/JJ_o = 1 - \Omega c_0$ is employed in equation (4.3). This identity comes from the first order term in ϵ of the linearization procedure of the constraint (2.1).

where h' denotes the first order derivative of $h(J_d)$ with respect to its argument. [3]

(b) Incremental dissipation inequality

Once performed the incremental analysis of the external work and of the time rate of the free energy, we formulate the incremental thermodynamics. We require that the incremental problem is consistent with the dissipation inequality enforcing it up to $O(\epsilon^2)$:

$$\mathcal{W}(\mathcal{P}) - \frac{d}{dt}\int_{\mathcal{P}} \frac{1}{JJ_o}(\psi_e + \psi_m)\, dV \geq 0\,, \quad \mathcal{P} \subset \mathcal{B}\,, \tag{4.11}$$

along with any incremental process. By using the aforementioned approximations for both the work and the free energy density up to $O(\epsilon^2)$, i.e. equations (4.7), (4.9) and (4.10), the incremental version of the dissipation inequality takes the form:

$$\begin{aligned} &\epsilon\left(\mathbf{S}_0 + \frac{\mu_e}{\Omega}\mathbf{I} - \frac{RT}{\Omega}h'(JJ_o)\mathbf{I} - \frac{G}{JJ_o}\mathbf{F}\mathbf{F}_o(\mathbf{F}\mathbf{F}_o)^T\right)\cdot\dot{\mathbf{H}} + \\ &\epsilon^2\left(\tilde{\mathbf{S}} + \frac{\tilde{\mu}}{\Omega}\mathbf{I} - \frac{RT}{\Omega}\Big(JJ_o h''(JJ_o)(\mathbf{I}\cdot\mathbf{H})\mathbf{I} + h'(JJ_o)((\mathbf{I}\cdot\mathbf{H})\mathbf{I} - \mathbf{H}^T)\Big)\right. \\ &\left. + \frac{\mu_e}{\Omega}((\mathbf{I}\cdot\mathbf{H})\mathbf{I} - \mathbf{H}^T) - \frac{G}{JJ_o}\mathbf{H}\mathbf{F}\mathbf{F}_o(\mathbf{F}\mathbf{F}_o)^T\right)\cdot\dot{\mathbf{H}} - \epsilon^2\left(\tilde{\mathbf{h}}\cdot\nabla\tilde{\mu}\right) \geq 0\,. \end{aligned} \tag{4.12}$$

The term of first order in ϵ in the incremental dissipation inequality (4.12) (first line) is identical to zero, as it can be easily verified by using equations (4.1) and (3.4). The terms of second order in ϵ in the incremental dissipation inequality (4.12) (second and third lines) are the approximation of the dissipation inequality obtained by applying the incremental theory and can be roughly rewritten as:

$$\left(\tilde{\mathbf{S}} - \mathcal{F}(\mathbf{F}, \mathbf{F}_o, \mu_e, h'(JJ_o), h''(JJ_o), \mathbf{H}) + \frac{\tilde{\mu}}{\Omega}\mathbf{I}\right)\cdot\mathbf{H} - \tilde{\mathbf{h}}\cdot\nabla\tilde{\mu} \geq 0\,. \tag{4.13}$$

The incremental theory is thermodynamically consistent, that is, following [25], the dissipation inequality is satisfied along any incremental process [26–28]. Moreover, we also assume that the dissipative components are only related to the diffusion problem and take

$$\tilde{\mathbf{S}} = \mathcal{F}(\mathbf{F}, \mathbf{F}_o, \mu_e, h'(JJ_o), h''(JJ_o), \mathbf{H}) - \frac{\tilde{\mu}}{\Omega}\mathbf{I} \quad \text{and} \quad \tilde{\mathbf{h}} = -\tilde{\mathbf{M}}\nabla\tilde{\mu}\,, \tag{4.14}$$

being the mobility $\tilde{\mathbf{M}}$ a positive definite tensor. So, the incremental stress depends on both the reference state $\mathcal{B}$ through the list $l_{\mathcal{B}} = (\mathbf{F}, \mathbf{F}_o, \mu_e, h'(JJ_o), h''(JJ_o))$ and the incremental deformation through $\mathbf{H}$. On the other hand, the incremental flux is assumed as depending on the reference state $\mathcal{B}$ through the mobility tensor $\tilde{\mathbf{M}}$ which may depend on the list $l_{\mathcal{B}}$ and must be positively definite. Little manipulations allow to simplify the representation of $\mathcal{F}(\mathbf{F}, \mathbf{F}_o, \mu_e, h'(JJ_o), h''(JJ_o), \mathbf{H})$ and write the incremental stress $\tilde{\mathbf{S}}$ as:

$$\tilde{\mathbf{S}} = \mathbb{C}[\mathbf{H}] - \tilde{p}\mathbf{I}\,, \tag{4.15}$$

being $\tilde{p} = \tilde{\mu}/\Omega$ usually defined as the pore pressure in the poroelastic theory [18], and where the incremental elasticity tensor $\mathbb{C}$ is defined as

$$\mathbb{C}[\mathbf{H}] = \frac{G}{JJ_o}\mathbf{H}\mathbf{B}_0 + \frac{1}{\Omega}(\mu_e - \mu(JJ_o))(\mathbf{H}^T - (\mathbf{I}\cdot\mathbf{H})\mathbf{I}) + \frac{RT}{\Omega}JJ_o h''(JJ_o)(\mathbf{I}\cdot\mathbf{H})\mathbf{I}\,, \tag{4.16}$$

being $\mathbf{B}_0 = (\mathbf{F}\mathbf{F}_o)(\mathbf{F}\mathbf{F}_o)^T$ the right Cauchy-Green strain tensor corresponding to the deformation of gradient $\mathbf{F}\mathbf{F}_o$. It is worth to note that the second term in equation (4.16), that is $\mu_e - \mu(JJ_o)$, is

[3] That derivative is evaluated at $\epsilon = 0$, that is when $\tilde{\mathbf{F}} = \mathbf{I} + \epsilon\mathbf{H} = \mathbf{I}$, therefore $J_d = \tilde{J}JJ_o = JJ_o$, as follows:

$$h'(JJ_o) = \frac{dh(J_d)}{dJ_d}\Big|_{J_d = JJ_o}$$

.

obtained – by using the equations (3.4), $(2.6)_2$, $(2.14)_2$ and (4.1) – as follows:

$$\frac{1}{\Omega}\left(\mu_e - \mu(JJ_o)\right) = \frac{1}{\Omega}\left(\mu_e - RTh'(JJ_o)\right) = p_0 = \frac{1}{3}\,\mathbf{I}\cdot\left(\frac{G}{JJ_o}\mathbf{B}_0 - \mathbf{S}_0\right). \tag{4.17}$$

Finally, the balance laws for the incremental chemo-mechanical problem are

$$\mathtt{div}\,\tilde{\mathbf{S}} = 0 \quad \text{and} \quad \dot{\gamma} = -\mathtt{div}\,\tilde{\mathbf{h}} \quad \text{in } \mathcal{B}\,, \tag{4.18}$$

which can be solved by considering suitable chemical and mechanical boundary conditions.

(c) General reduced models

In order to validate the proposed incremental theory, we show that two well known problems in literature, namely (i) the classic linear poroelastic theory [18,21], and (ii) the standard incremental problem of elasticity around a stressed state [29], can be derived as two limit cases.

Poroelastic theory

The classic poroelastic theory [18] can be viewed as an incremental problem from a stress-free reference configuration [21]. Correspondingly, our problem may be viewed as a prestressed form of the classic poroelastic theory which, to the authors' best knowledge, has been not yet proposed within the scientific community. When the prestress is zero, i.e. $\mathbf{S}_0 = 0$, the configuration $\mathcal{B}$ is stress-free. Therefore, $k = k_\perp = 0$ or, equivalently, $\mathcal{B} \equiv \mathcal{B}_o$. With this, $\mathbf{F}_o = \lambda_o\mathbf{I}$ and $\mathbf{F} = \mathbf{I}$, and the incremental deformation process $\tilde{\mathbf{F}} = \mathbf{F}_d\mathbf{F}_o^{-1}$ brings $\mathcal{B}_o$ to $\mathcal{B}_t$.
According to the aforementioned assumptions, the equation (4.15) is reduced to:

$$\begin{aligned}\tilde{\mathbf{S}} &= \frac{G}{\lambda_o}\mathbf{H} + \frac{G}{\lambda_o}\mathbf{H}^T - \left(\frac{RT}{\Omega}J_o h''(J_o) + \frac{G}{\lambda_o}\right)(\mathbf{I}\cdot\mathbf{H})\mathbf{I} - \tilde{p}\mathbf{I} \\ &= 2G\mathbf{E} + \left(K - \frac{2}{3}G\right)(\mathbf{I}\cdot\mathbf{E})\mathbf{I} - \tilde{p}\mathbf{I}\,,\end{aligned} \tag{4.19}$$

where equation (4.17) is employed, and where $\mathbf{H}\cdot\mathbf{I} = \mathbf{E}\cdot\mathbf{I}$ with $\frac{1}{2}\mathbf{H} + \mathbf{H}^T = \mathbf{E}$, while G and K are the poroelastic shear and bulk moduli defined as in Ref. [21].

Residual stress in an elastic body

When the chemical field due to solvent transport is neglected, i.e. when only the mechanical field is considered, our incremental problem reduces to the elastic incremental problem with respect to a prestressed configuration, as in Ref. [29]. Indeed, the dissipation inequality (4.12) reduces to:

$$\epsilon\left(\mathbf{S}_0 - \frac{G}{JJ_o}\mathbf{F}\mathbf{F}_o(\mathbf{F}\mathbf{F}_o)^T\right)\cdot\dot{\mathbf{H}} + \epsilon^2\left[\tilde{\mathbf{S}} - \frac{G}{JJ_o}\mathbf{H}\mathbf{F}\mathbf{F}_o(\mathbf{F}\mathbf{F}_o)^T\right]\cdot\dot{\mathbf{H}} \geq 0\,. \tag{4.20}$$

Again, the term of first order in ϵ is identically zero, as it can be verified from the constitutive equation (4.1) for $\mathbf{S}_0$ (the material is assumed compressible, hence $p_0 = 0$). The term of second order in ϵ delivers the incremental stress $\tilde{\mathbf{S}}$. All in all, it holds:

$$\mathbf{S} = \mathbf{S}_0 + \epsilon\tilde{\mathbf{S}} = \mathbf{S}_0 + \epsilon\frac{G}{JJ_o}\mathbf{H}\mathbf{F}\mathbf{F}_o(\mathbf{F}\mathbf{F}_o)^T = \mathbf{S}_0 + \epsilon\mathbb{C}[\mathbf{H}]\,. \tag{4.21}$$

In this case, it is useful to additively decompose the increment $\mathbf{H}$ of the deformation gradient $\tilde{\mathbf{F}}$ in the standard symmetric and skew-symmetric part, $\mathbf{E}$ and $\mathbf{W}$, respectively, as $\mathbf{H} = \mathbf{E} + \mathbf{W}$ and show that

$$\mathbb{C}[\mathbf{W}] = \mathbf{W}\mathbf{S}_0, \quad \mathrm{skw}\,\mathbb{C}[\mathbf{E}] = \frac{1}{2}\left(\mathbf{E}\mathbf{S}_0 - \mathbf{S}_0\mathbf{E}\right), \quad \text{and} \quad \mathrm{sym}\,\mathbb{C}[\mathbf{E}] = \mathbb{C}[\mathbf{E}]\,. \tag{4.22}$$

By inserting the previous formulas (4.22) into equation (4.21), the reference stress $\mathbf{S}$ takes the same form as in the work of Hoger [29]:

$$\mathbf{S} = \mathbf{S}_0 + \epsilon(\mathbf{W}\mathbf{S}_0 + \mathbb{C}[\mathbf{E}] + \frac{1}{2}\left(\mathbf{E}\mathbf{S}_0 - \mathbf{S}_0\mathbf{E}\right))\,. \tag{4.23}$$

5. Incremental problem

In this section, the general incremental analysis presented in Section 4, is applied to a one-dimensional time-dependent problem in order to derive a closed-form solution and investigate the effects of the prestress on the main chemo-mechanical variables.
The unknown fields which completely determine the incremental gel dynamics are the incremental displacement field $\mathbf{u}$, and the incremental concentration field γ. These variables satisfy the balance equation of forces

$$\mathrm{div}\,\tilde{\mathbf{S}} = \mathbf{0} \quad \text{with} \quad \tilde{\mathbf{S}} = \mathbb{C}[\mathbf{H}] - \tilde{p}\mathbf{I}\,, \quad \text{and} \tag{5.1}$$

the balance equation of solvent mass

$$\dot{\gamma} = -\mathrm{div}\,\tilde{\mathbf{h}} \quad \text{with} \quad \tilde{\mathbf{h}} = -\tilde{\mathbf{M}}\nabla\tilde{\mu} = -\tilde{\mathbf{M}}\nabla\Omega\tilde{p}\,, \tag{5.2}$$

respectively. Moreover, the two unknown fields are coupled through the linearized expression of the volumetric constraint within the incremental framework:

$$\Omega\gamma = \mathbf{I}\cdot\mathbf{H}\,. \tag{5.3}$$

The initial and boundary conditions of the differential system identified by the equations (5.1)–(5.3), depend on the particular configuration investigated.

One-dimensional model

With the aim of appreciating the differences induced by the compressive or tensile prestressed states in the reference configuration $\mathcal{B}$, we consider a one-dimensional problem already discussed analytically and experimentally by Doi [11] and Yoon et al. [20]. Therein, a linear poroelastic theory for a stress-free reference configuration is employed to investigate a thin gel sheet which (i) is glued to a rigid impermeable wall of unit normal $\mathbf{e}_3$ at its bottom surface ($x_3 = -h$) and (ii) is free at its top surface ($x_3 = 0$) (see figure 7). Furthermore, in [20] experimental observations have been used to validate the performed analytical investigations. In the following, the same problem is discussed by using our linear poroelastic theory for a prestressed configuration. It is worth noting that, for this particular case, the diffusion and the elastic problem can be solved sequentially.

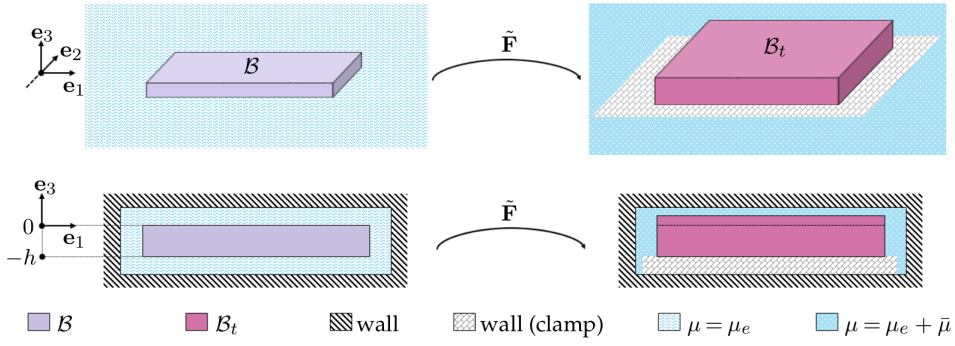

Figure 7. Prestressed thin gel sheet clamped at its bottom surface ($x_3 = -h$) and free at its top surface ($x_3 = 0$). A change in the bath's chemical potential from μ_e (blue pattern) to $\mu_e + \bar{\mu}$ (dark blue pattern) determines the incremental problem described by the deformation $\tilde{\mathbf{F}}$.

As the in-plane dimensions of the gel are much larger than its thickness, it is assumed that solvent is driven inside/outside the gel mostly from its top surface once a change $\bar{\mu}$ in the chemical potential μ_e occurs. Therefore, the incremental flux shows only a component in the $\mathbf{e}_3$ direction, which is a function of the thickness coordinate x_3 and of the time t: $\tilde{\mathbf{h}} = h_3(x_3, t)\mathbf{e}_3$. The same property holds for the incremental potential $\tilde{\mu} = \tilde{\mu}(x_3, t)$ due to the Darcy's law $(5.2)_2$, as well

as for all the fields involved in the analysis. Moreover, as the sheet is thin, the only meaningful component of the displacement vector $\mathbf{u}$ is the component normal to the wall:

$$\mathbf{u} = \hat{\mathbf{u}} + w\mathbf{e}_3\,, \quad \text{with} \quad w = w(x_3, t) \quad \text{and} \quad \hat{\mathbf{u}} \equiv \mathbf{0}\,, \tag{5.4}$$

with $\hat{\mathbf{u}} = u\mathbf{e}_1 + v\mathbf{e}_2$ the two in-plane components of the incremental displacement field. The incremental stress $\tilde{\mathbf{S}} = \tilde{\mathbf{S}}(x_3, t)$ can be written in terms of its in-plane and out-of-plane components as $\tilde{\mathbf{S}} = \tilde{\sigma}\hat{\mathbf{I}} + \tilde{\sigma}_{33}\mathbf{e}_3 \otimes \mathbf{e}_3$. According to the aforementioned assumptions and by using the expression (4.15), it holds:

$$\tilde{\sigma} = \mathcal{Q}(\lambda_o, \lambda, \lambda_\perp)\varepsilon_{33} - \tilde{p}\,, \quad \text{and} \quad \tilde{\sigma}_{33} = \mathcal{A}(\lambda_o, \lambda, \lambda_\perp)\varepsilon_{33} - \tilde{p}\,, \tag{5.5}$$

with $\mathbf{H} \cdot \mathbf{e}_3 \otimes \mathbf{e}_3 = \varepsilon_{33} = \partial w/\partial x_3$ the deformation in the thickness direction, and where

$$\mathcal{Q}(\lambda_o, \lambda, \lambda_\perp) = \left(-p_0 + \frac{RT}{\Omega} JJ_o h''(JJ_o)\right)\,, \text{and} \tag{5.6}$$

and

$$\mathcal{A}(\lambda_o, \lambda, \lambda_\perp) = \left(\frac{G}{JJ_o}\lambda_o^2\lambda_\perp^2 + \frac{RT}{\Omega} JJ_o h''(JJ_o)\right) \tag{5.7}$$

are two functions which are fully defined by the solution of the reference stressed state $\mathcal{B}$, previously discussed.
The balance of forces (5.1) prescribes that $\tilde{\sigma}_{33,3}(x_3, t) = 0$ and can be solved by using the boundary condition of free stress at the tip, i.e. $\tilde{\sigma}_{33}(0, t) = 0$. Therefore, by using equation $(5.5)_2$, it holds that

$$\tilde{\sigma}_{33} = 0 \qquad \Rightarrow \qquad \mathcal{A}(\lambda_o, \lambda, \lambda_\perp)\varepsilon_{33} = \tilde{p}\,. \tag{5.8}$$

It is useful to introduce an incremental in-plane resultant force per unit length $\tilde{F}(t)$:

$$\tilde{F}(t) = \int_{-h}^{0} \tilde{\sigma}(x_3, t)\, dx_3 = (\mathcal{Q} - \mathcal{A}) \int_{-h}^{0} \varepsilon_{33}(x_3, t)\, dx_3\,, \tag{5.9}$$

where, in the last step, equations $(5.5)_1$ and $(5.8)_2$ are employed. The integration of equation (5.9), together with the clamp boundary condition $w(-h, t) = 0$, gives an expression for the incremental tip displacement which corresponds to the change in thickness of the sheet:

$$w(0, t) = \frac{\tilde{F}(t)}{\mathcal{Q} - \mathcal{A}}\,. \tag{5.10}$$

In steady-state, when $t = \bar{t}$, the incremental chemical potential inside the gel is the same of the surrounding environment, that is $\tilde{\mu}(x_3, \bar{t}) = \Omega\tilde{p}(x_3, \bar{t}) = \bar{\mu}$. Therefore, the integration of the equation $(5.8)_2$ in steady-state conditions gives the following expression of the stationary incremental tip displacement:

$$\int_{-h}^{0} \varepsilon_{33}(x_3, \bar{t})\, dx_3 = \frac{1}{\mathcal{A}} \int_{-h}^{0} \tilde{p}(x_3, \bar{t})\, dx_3 \qquad \Rightarrow \qquad w(0, \bar{t}) = \frac{h}{\mathcal{A}\Omega}\bar{\mu}\,. \tag{5.11}$$

Equations (5.10) and $(5.11)_2$ share the same structure like the ones in [20], even though the different denominators take into account the different reference configuration adopted in our research, which is not stress-free and reached through two steps: (i) a stress-free step $\mathbf{F}_o$, and (ii) a constrained not stress-free step $\mathbf{F}$. It is worth noting that in [20] the reference configuration of the incremental problem is reached through a one-step and stress-free deformation process which is named as $\mathbf{F}_{oo} = \lambda_{oo}\mathbf{I}$ in this work.
A comparison between the tip displacement in steady-state conditions of the proposed model $w(0, \bar{t})$, see equation (5.11), with the one presented in [20] $w_Y(0, \bar{t})$ is discussed. The displacement

ratio and the relative change of the displacement are:

$$\frac{w(0,\bar{t})}{w_Y(0,\bar{t})} = \frac{3K_{oo}+4G_{oo}}{3\mathcal{A}}\,, \quad \text{and} \quad \Upsilon = \frac{w(0,\bar{t})-w_Y(0,\bar{t})}{w_Y(0,\bar{t})}\,, \tag{5.12}$$

being G_{oo} and K_{oo} the classical poroelastic shear and bulk moduli [21], respectively, defined as:

$$G_{oo} = \frac{G}{\lambda_{oo}}\,, \quad \text{and} \quad K_{oo} = \frac{RT}{\Omega} J_{oo} h''(J_{oo}) - \frac{1}{3} G_{oo}\,, \tag{5.13}$$

where $J_{oo} = \lambda_{oo}^3$, with λ_{oo} the stretch related to the deformation process $\mathbf{F}_{oo} = \lambda_{oo}\mathbf{I}$ which identifies the reference stress-free configuration in [20]. The parameter λ_{oo} is evaluated through equation (2.13) as a solution of the free swelling problem induced by $\mu = \mu_{oo}$:

$$\mu(J_{oo}) + \frac{G}{\lambda_{oo}}\,\Omega = \mu_{oo}\,, \tag{5.14}$$

with $\mu_{oo} = \mu_e$ in order to have a consistent comparison within equations (5.12).
The isolines of the relative change of the displacement Υ are expressed as percentages in figure 8(A) for a reference state with elastic constraints along the thickness direction (case (i) developed in Section 3 when $k = 0$), and in figure 8(B) for a reference state with plane elastic constraints (case (ii) developed in Section 3 when $k_\perp = 0$). A point of the isoline corresponds to a particular choice of $\mu_e, \alpha_\perp$ and μ_e, α for each case, respectively.

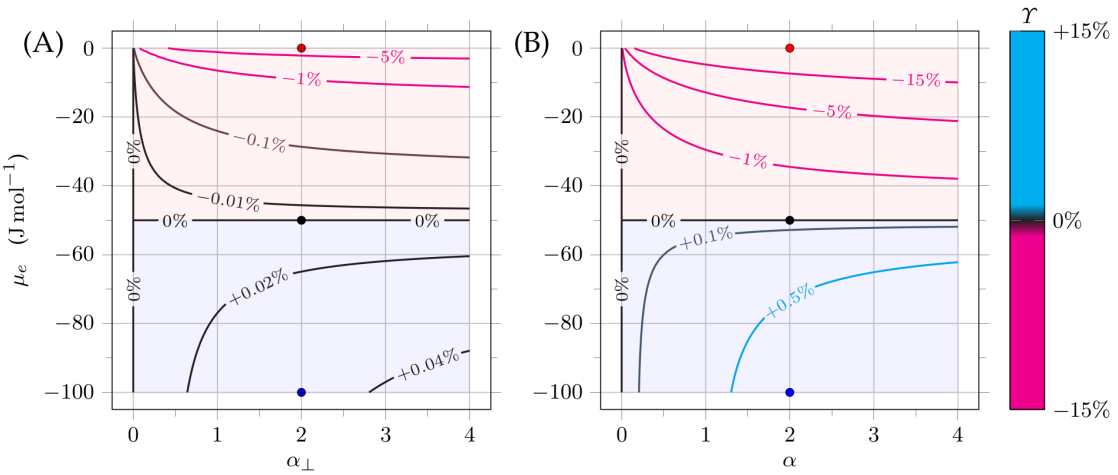

Figure 8. (A) Isolines Υ for a reference state with elastic constraints along the thickness direction $k = 0$. (B) Isolines Υ for a reference state with plane elastic constraints $k_\perp = 0$. Large values of Υ are identified by cyan solid isolines, while low values by magenta solid isolines. The red, black, and blue dots correspond to the same states.

Large tip displacements $w(0,\bar{t})$ with respect to $w_Y(0,\bar{t})$ are represented by cyan solid isolines (positive percentages). Otherwise, small tip displacements $w(0,\bar{t})$ with respect to $w_Y(0,\bar{t})$ are represented by magenta solid isolines (negative percentages). Zero relative changes of the displacement (black isolines), that is $\Upsilon = 0\%$, are achieved for $\mu_e = \mu_o$, for any values of $\alpha_\perp$ or α (horizontal black isoline), and for $\alpha_\perp = 0$ or $\alpha = 0$, for any values of μ_e (vertical black isoline). Under these conditions in both cases, the one presented in [20] and the one here discussed, the reference configuration is stress-free, thus determining the same tip displacements $w(0,\bar{t}) = w_Y(0,\bar{t})$. As expected, the gel reaches lower tip displacements than the one in Ref. [20] when a compressive prestress (light red zone) is present. Vice versa, the gel reaches larger tip displacements when a tensile prestress (light blue zone) is present. Finally, the behavior of the relative change is in accordance with the trend of the corresponding dimensionless stresses, i.e. $\sigma_\perp/G_o$ and σ/G_o, as shown in figures 4(B) and 5(B). It is worth noting that all the expressions presented in this section can be reduced to the standard poroelastic problem given in [20] by

substituting $\lambda = \lambda_\perp = 1$ and $\mathbf{S}_0 = 0$ in order to bring the problem back to a stress-free reference configuration, and by using the definitions given in equations (5.13). [4]
Finally, the time derivative of the volumetric constraint (5.3) is given by using equation $(5.8)_2$:

$$\Omega\,\gamma = \mathbf{I}\cdot\mathbf{H} = \varepsilon_{33} \qquad \Rightarrow \qquad \Omega\,\dot{\gamma} = \frac{1}{\mathcal{A}}\,\dot{\tilde{p}} = \frac{1}{\mathcal{A}\Omega}\,\dot{\tilde{\mu}}\,. \tag{5.15}$$

Equation $(5.15)_2$ can be substituted in the one-dimensional balance equation for the solvent, that is equation (5.2), in order to obtain a partial differential equation in space and time for the incremental chemical potential $\tilde{\mu}$:

$$\dot{\tilde{\mu}} = D\frac{\partial}{\partial x_3}\left(\frac{\partial\tilde{\mu}}{\partial x_3}\right) \quad \text{with} \quad D = \tilde{M}\mathcal{A}\Omega^2\,, \tag{5.16}$$

where the mobility is defined as $\tilde{M} = \kappa(\eta\Omega^2)^{-1}$, with κ ($[\kappa] = \mathrm{m}^2$) the permeability of the gel and η ($[\eta] = \mathrm{Pa\,s}$) the viscosity of the solvent.
Equation (5.16) takes the familiar form of the diffusion equation, with D a constant parameter whose unit of measures equals the ones of a diffusivity coefficient. Equation (5.16) can be solved once suitable initial and boundary conditions are imposed. At the initial state the incremental potential is zero: $\tilde{\mu}(x_3, 0) = 0$. At the top surface, the incremental chemical potential equals that of the surrounding environment: $\tilde{\mu}(0, t) = \bar{\mu}$. Finally, at the bottom surface, the impermeable condition holds: $\mathbf{n}\cdot\nabla\tilde{p} = \mathbf{n}\cdot\nabla\tilde{\mu}/\Omega = 0$, being $\mathbf{n}$ an outward normal in the $\mathbf{e}_3$ direction. This condition in a one-dimensional context becomes $\partial\tilde{\mu}(-h, t)/\partial x_3 = 0$. The complete analytical solution, in space and time, for $\tilde{\mu}(x_3, t)$ is obtained by using the approach of the separation of variables for non-homogeneous boundary conditions which leading to:

$$\tilde{\mu}(x_3, t) = \bar{\mu} + \frac{4\bar{\mu}}{\pi}\sum_{n=0}^{\infty}\frac{1}{2n+1}\exp\left(-\frac{Dt\pi^2(2n+1)^2}{4h^2}\right)\sin\left(\frac{x_3\pi(2n+1)}{2h}\right)\,. \tag{5.17}$$

Then, the profiles of all the other chemo-mechanical variables can be determined according to the previous relations: $\tilde{p}(x_3, t)$, $\epsilon_{33}(x_3, t)$, $\gamma(x_3, t)$, $\tilde{\sigma}(x_3, t)$ and $\tilde{\sigma}_{33}(x_3, t)$.
In particular, we are interested in the time evolution of the incremental in-plane resultant force per unit length $\tilde{F}(t)$ given in equation (5.9). By combining the latter equation with equation $(5.8)_2$, being aware that $\tilde{p} = \tilde{\mu}/\Omega$, it follows that

$$\tilde{F}(t) = \frac{(\mathcal{Q}-\mathcal{A})}{\mathcal{A}\Omega}\int_{-h}^{0}\tilde{\mu}(x_3, t)\,dx_3\,. \tag{5.18}$$

Once the integration along the thickness direction of $\tilde{\mu}(x_3, t)$ is performed, in accordance with the expression (5.17), an explicit equation for $\tilde{F}(t)$ is obtained:

$$\tilde{F}(t) = \frac{(\mathcal{Q}-\mathcal{A})\bar{\mu}h}{\mathcal{A}\Omega}\left(1 - \frac{8}{\pi^2}\sum_{n=0}^{\infty}\frac{1}{(2n+1)^2}\exp\left(-\frac{Dt\pi^2(2n+1)^2}{4h^2}\right)\right)\,. \tag{5.19}$$

It is worth to note that the total resultant force per unit length $F(t)$ can be obtained by integrating the total in-plane stress which includes the prestress:

$$F(t) = \int_{-h}^{0}(\sigma + \tilde{\sigma}(x_3, t))\,dx_3 = F_0 + \tilde{F}(t)\,, \quad \text{with} \quad F_0 = \sigma h\,, \tag{5.20}$$

where $F_0 = 0$ for a reference configuration $\mathcal{B}$ with elastic constraints along the thickness ($\sigma = 0$).
In order to represent $\tilde{F}(t)$, further parameters have to be introduced, namely: the incremental chemical potential in steady-state $\bar{\mu} = -1\ \mathrm{J\,mol^{-1}}$ which is in accordance with the assumptions of small incremental problem, the thickness of the membrane $h = 5\times10^{-4}$ m, the permeability

[4] The reduction of the proposed model to a stress-free reference configuration, gives that

$$\mathcal{A} = \frac{4}{3}G_{oo} + K_{oo} \quad \text{and} \quad \mathcal{Q} = -\frac{2}{3}G_{oo} + K_{oo}\,.$$

of the gel $\kappa = 1 \times 10^{-18}$ m^2, and the viscosity of the solvent $\eta = 0.2$ Pa s. [5] A recap of these parameters is given in Table 2. Moreover, the parameters $\mathcal{Q}$ and $\mathcal{A}$ depend on λ and $\lambda_\perp$ (i.e. on to the particular state of the reference configuration $\mathcal{B}$), as shown in equations (5.6) and (5.7).

Table 2. Parameters introduced for the investigation of $\tilde{F}(t)$ which are in accordance with Ref. [21].

Parameter	Value	Unit
$\bar{\mu}$	-1	J mol^{-1}
h	5×10^{-4}	m
κ	1×10^{-18}	m^2
η	0.2	Pa s

The time evolution of the in-plane resultant force per unit length $\tilde{F}(t)$ is shown in figure 9(A). The investigation only deals with the case (i) developed in Section 3 where the reference configuration $\mathcal{B}$ has elastic constraints along the thickness direction ($k = 0$). According to equation $(5.20)_1$, only in this situation, the incremental resultant force equals the total resultant force, being the in-plane prestress zero. Among all the possible states of $\mathcal{B}$, described by the couples $(\lambda, \lambda_\perp)$ in figure 4(A), only the benchmark states identified by $\alpha_\perp = 2$, with $\mu_e = 0$ J mol^{-1} (red solid line), $\mu_e = -50$ J mol^{-1} (black solid line), and $\mu_e = -100$ J mol^{-1} (blue solid line), will be taken into account. These states represent a reference configuration in pre-compression, stress-free, and in pre-tension, respectively. Throughout the manuscript, they are identified by red, black, and blue crossed dots. A parametric investigation for the solvent viscosity η and the gel permeability κ is shown in figure 9(B) starting from the case with $\mu_e = -50$ J mol^{-1} (black solid line).

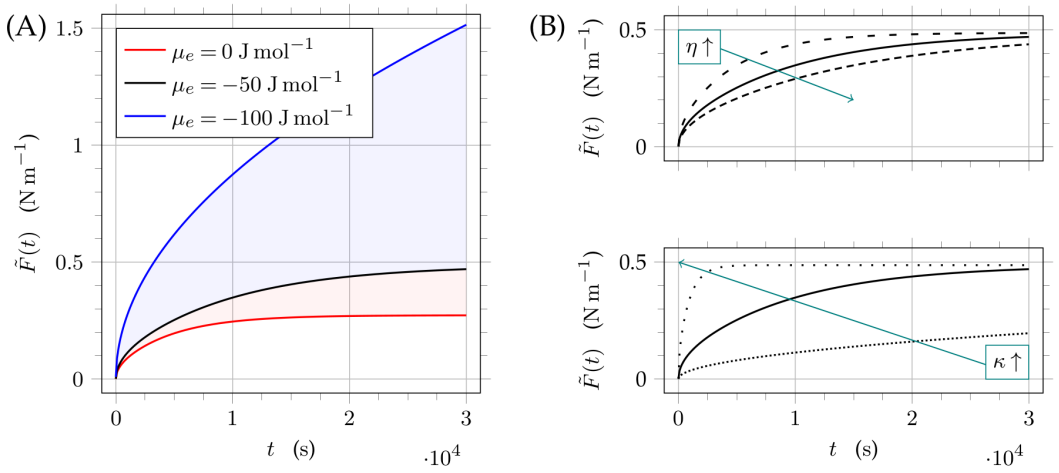

Figure 9. (A) Time evolution of the in-plane resultant force per unit length $\tilde{F}(t)$. A reference configuration with elastic constraints along the thickness direction is taken into account, with different values of μ_e: 0 J mol^{-1} (red solid line), -50 J mol^{-1} (black solid line), -100 J mol^{-1} (blue solid line). The light blue and light red areas identify the tension and the compression zones related to the prestress. (B) Parametric investigation on $\tilde{F}(t)$ for the case $\mu_e = -50$ J mol^{-1} (black solid line). The parameters analyzed are the solvent viscosity η, with $\eta = 0.1, 0.2, 0.3$ Pa s, and the gel permeability κ, with $\kappa = 1 \times 10^{-19}, 1 \times 10^{-18}, 1 \times 10^{-17}$ m^2.

In figure 9(A), the parameter $\bar{\mu}$ is fixed to $\bar{\mu} = -1$ J mol^{-1}. When the chemical potential decreases with respect to its equilibrium value ($\mu_e + \bar{\mu} < \mu_e$) the gel reduces its volume, expels solvent and undergoes tension, therefore $\tilde{F}(t) > 0$ for each of the value of μ_e taken into account. Equation (5.19) clearly shows that when $\bar{\mu} = 1$ J mol^{-1} the opposite behavior $\tilde{F}(t) < 0$ is described, being $\bar{\mu}$

[5] The parameters h, κ and η are chosen in accordance with the work of Lucantonio et al. [21], even though they have the same order of magnitude as in the work of Yoon et al. [20].

only a multiplicative factor for $\tilde{F}(t)$. The exponential term in equation (5.19) regulates the speed at which steady-state conditions are achieved. The coefficient of the exponential term depends on $D = D(\mathcal{A})$ with $\mathcal{A} = \mathcal{A}(\lambda, \lambda_\perp)$. Steady-state conditions are reached faster when the gel has a compressive prestress (red solid line) with respect to the case of a tensile prestress (blue solid line). Indeed, the values of λ and $\lambda_\perp$ are larger for $\mu_e = 0$ J mol^{-1}, see the red crossed dot in figure 4(A), with respect to the values of λ and $\lambda_\perp$ for $\mu_e = -50, -100$ J mol^{-1}, see the black and blue crossed dots in figure 4(A). Therefore, when $\mu_e = 0$ J mol^{-1}, the larger coefficient of the exponential factor brings the gel faster towards the equilibrium. As expected, for a particular instant in time, $\tilde{F}(t)$ shows low values for a compressive prestress (red solid line) with respect to a tensile prestress (blue solid line): the compressive prestress acts, in the thickness direction, against the trend of the gel to generate a positive stress. Furthermore, the light blue and the light red areas identify, as before, the tension and compression zones, delimiting all the solutions for -100 J mol$^{-1} \leq \mu_e < -50$ J mol^{-1}, and for -50 J mol$^{-1} < \mu_e \leq 0$ J mol^{-1}, respectively.
The influence of the solvent viscosity η and of the gel permeability κ is investigated in figure 9(B) for the case $\mu_e = -50$ J mol^{-1} (black solid line), and by keeping fixed all the other parameters. Obvious conclusions can be obtained by analyzing the equation (5.19). The parameters η and κ only affect the exponential term, therefore the steady-state solution remains the same. As expected, larger viscosity η (black densely dashed lines) and lower permeability κ (black densely dotted lines) behave the same way: steady-state conditions are achieved slower. Finally, the influence of the thickness of the gel h, which is not given in figure, can be discussed by observing that h influences the steady-state solution, being present in the factor of the exponential, and the speed of the gel to reach steady-state conditions, being present in the coefficient of the exponential.

6. Conclusions and outlook

In the present research, two main topics results are discussed.
First, the nonlinear stress-diffusion model is employed to investigate the stress state arising in constrained hydrated polymer gels when a change in the chemical potential leads to swelling or shrinking. The constraints are represented by a set of elastic springs mimicking homogeneous mechanical confinements. It is shown that swelling induced deformations and stresses develop according to the boundary conditions of the problem: (i) the initial and the final chemical potential, and (ii) the stiffness of the mechanical constraints. A parametric investigation is performed considering two limiting cases with elastic constraints just along (i) the out-of-plane direction, and (ii) the in-plane constraints. The performed analysis can be potentially exploited to study all kinds of problems in which boundary effects are induced by other bodies, e.g. the effects generated by other layers on a single membrane in a fuel cell stack.
Second, an incremental theory for stress-diffusion starting from a prestressed reference state is developed in a thermodynamically consistent way. The proposed model can be viewed as a linear poroelastic theory for prestressed configurations, which has not yet been presented within the scientific community. A validation of the proposed formulation is accomplished by a comparison with two limiting cases already discussed in literature. As expected, the linearized equation of the incremental stress depends on the state of the reference configuration: in particular it depends on (i) the prestress, (ii) the initial stretch of the membrane, and on (iii) the difference between the reference and the final chemical potential. As a benchmark problem, the incremental dynamics of a thin plate-like gel body from a prestressed reference state is studied, and time-dependent one-dimensional closed form solution is obtained. The outcomes of the analysis have been compared with the observations already performed in literature on stress-free gels. The expected behavior is correctly described by the proposed model. Furthermore, a parametric investigation allows to understand the influence on the solution of the main material parameters.
In this article, we restricted the discussion to problems that can be treated by analytical calculations. However, the model and the analysis presented in the proposed paper, are a first step towards a future study which aims at comprehending the multiphysics problem of thin ion-exchange membranes when a difference in voltage is applied between the two ends of the

plate. Hydrated polymeric membranes made of Nafion are widely employed in fuel cells and rechargeable batteries. These membranes show an electro-chemo-hydro-mechanical fully coupled behavior, which can be modeled by extending our model. Likewise, the same incremental model can be developed to describe other multiphysics behavior of materials which have been already extensively studied in literature, e.g. ionic-polymer-metal-composites [30–32], hydrogels [33,34], ferrogels [35], polymer membrane in electrochemical cells [36,37].

Finally, the proposed incremental theory for stress-diffusion starting from a stressed state can be used to explicitly investigate the stress and strain changes induced by a small alteration of the environmental conditions of polymer gels under uniaxial or biaxial stretching [38–40]. In this case, (i) the expected solution is non-homogeneous, as for non-homogeneous polymers, (ii) the compact results shown in this paper do not hold, and (iii) a full nonlinear analysis can be difficult while an appropriate incremental theory can deliver some interesting results.

Funding statement

This work was supported by the European Union (ERDF) and the Free State of Saxony via the ESF project 100231947 (Young Investigators Group "Computer Simulations for Materials Design - CoSiMa"), and by the Graduate Academy TU Dresden for the mobility grant within the program *great!*$_{ipid4all}$ (projects 2017_64 and 2018_84).

References

1. Burgert I, Fratzl P. 2009 Actuation systems in plants as prototypes for bioinspired devices. *Philosophical Transactions of the Royal Society A: Mathematical, Physical and Engineering Sciences* **367**(1893), 1541 – 1557.
2. Dai S, Ravi P, Tam KC. 2009 Thermo- and photo-responsive polymeric systems. *Soft Matter* **5**(13), 2513 – 2533.
3. Erb RM, Sander JS, Grisch R, Studart A. 2013 Self-shaping composites with programmable bioinspired microstructures. *Nature Communications* **4**(1712), 1 – 8.
4. Byun M, Santangelo CD, Hayward RC. 2013 Swelling-driven rolling and anisotropic expansion of striped gel sheets. *Soft Matter* **9**(34), 8264 – 8273.
5. Liu Y, Yong X, McFarlin G, Kuksenok O, Aizenberg J, Balazs AC. 2015 Designing a gel-fiber composite to extract nanoparticles from solution. *Soft Matter* **11**(44), 8692 – 8700.
6. Winstanley HF, Chapwanya M, McGuinness MJ, Fowler AC. 2010 A polymer–solvent model of biofilm growth. *Proceedings of the Royal Society A: Mathematical, Physical and Engineering Sciences* **467**(2129), 1449 – 1467.
7. Miyamoto N, Shintate M, Ikeda S, Hoshida Y, Yamauchi Y, Motokawa R, Annaka M. 2013 Liquid crystalline inorganic nanosheets for facile synthesis of polymer hydrogels with anisotropies in structure, optical property, swelling/deswelling, and ion transport/fixation. *Chemical Communications* **49**(11), 1082 – 1084.
8. Alberti G, Narducci R. 2009 Evolution of permanent deformations (or memory) in Nafion 117 membranes with changes in temperature, relative humidity and time, and its importance in the development of medium temperature PEMFCs. *Fuel Cells* **9**(4), 410 – 420.
9. Bai R, Yang J, Suo Z. 2019 Fatigue of hydrogels. *European Journal of Mechanics-A/Solids* **74**, 337 – 370.
10. Mao Y, Anand L. 2018 A theory for fracture of polymeric gels. *Journal of the Mechanics and Physics of Solids* **115**, 30 – 53.
11. Doi M. 2009 Gel Dynamics. *Journal of the Physical Society of Japan* **78**(5), 052001-1 – 052001-19.
12. Chester SA, Anand L. 2010 A coupled theory of fluid permeation and large deformations for elastomeric materials. *Journal of the Mechanics and Physics of Solids* **58**(11), 1879 – 1906.
13. Hong W, Zhao X, Zhou J, Suo Z. 2008 A theory of coupled diffusion and large deformation in polymeric gels. *Journal of the Mechanics and Physics of Solids* **56**(5), 1779 – 1793.
14. Lucantonio A, Nardinocchi P, Teresi L. 2013 Transient analysis of swelling-induced large deformations in polymer gels. *Journal of the Mechanics and Physics of Solids* **61**(1), 205 – 218.
15. Lucantonio A, Nardinocchi P, Pezzulla M. 2014 Swelling-induced and controlled curving in layered gel beams. *Proceedings of the Royal Society A: Mathematical, Physical and Engineering Sciences* **470**(2171), 20140467-1 – 20140467-16.

16. Nardinocchi P, Teresi L. 2016 Actuation performances of anisotropic gels. *Journal of Applied Physics* **120**(21), 215107-1 – 215107-10.
17. Nardinocchi P, Puntel E. 2017 Swelling-induced wrinkling in layered gel beams. *Proceedings of the Royal Society A: Mathematical, Physical and Engineering Sciences* **473**(2207), 20170454-1 – 20170454-17.
18. Biot MA. 1941 General theory of three-dimensional consolidation. *Journal of Applied Physics* **12**(2), 155 – 164.
19. Tanaka T, Fillmore DJ. 1979 Kinetics of swelling of gels. *The Journal of Chemical Physics* **70**(3), 1214 – 1218.
20. Yoon J, Cai S, Suo Z, Hayward RC. 2010 Poroelastic swelling kinetics of thin hydrogel layers: comparison of theory and experiment. *Soft Matter* **6**(23), 6004 – 6012.
21. Lucantonio A, Nardinocchi P. 2012 Reduced models of swelling-induced bending of gel bars. *International Journal of Solids and Structures* **49**(11-12), 1399 – 1405.
22. Kusoglu A, Karlsson AM, Santare MH, Cleghorn S, Johnson WB. 2007 Mechanical behavior of fuel cell membranes under humidity cycles and effect of swelling anisotropy on the fatigue stresses. *Journal of Power Sources* **170**(2), 345 – 358.
23. Flory PJ, Rehner J. 1943 Statistical Mechanics of Cross-Linked Polymer Networks I. Rubberlike Elasticity. *The Journal of Chemical Physics* **11**(11), 512 – 520.
24. Flory PJ, Rehner J. 1943 Statistical Mechanics of Cross-Linked Polymer Networks II. Swelling. *The Journal of Chemical Physics* **11**(11), 521 – 526.
25. Coleman BD, Noll W. 1963 The thermodynamics of elastic materials with heat conduction and viscosity. *Archive for Rational Mechanics and Analysis* **13**(1), 167 – 178.
26. Nardinocchi P, Pezzulla M, Placidi L. 2011 Thermodynamically based multiphysic modeling of ionic polymer metal composites. *Journal of Intelligent Material Systems and Structures* **22**(16), 1887 – 1897.
27. Galante S, Lucantonio A, Nardinocchi P. 2013 The multiplicative decomposition of the deformation gradient in the multiphysics modeling of ionic polymers. *International Journal of Non-Linear Mechanics* **51**, 112 – 120.
28. Rossi M, Wallmersperger T, Ramirez JA, Nardinocchi P. 2018 Thermodynamically consistent electro-chemo-mechanical model for polymer membranes. *Electroactive Polymer Actuators and Devices (EAPAD) XX. Proceedings of SPIE* **10594**, 105940K-1 – 105940K-11.
29. Hoger A. 1986 On the determination of residual stress in an elastic body. *Journal of Elasticity* **16**(3), 303 – 324.
30. Porfiri M. 2008 Charge dynamics in ionic polymer metal composites. *Journal of Applied Physics* **104**(10), 104915-1 – 104915-10.
31. Del Bufalo G, Placidi L, Porfiri M. 2008 A mixture theory framework for modeling the mechanical actuation of ionic polymer metal composites. *Smart Materials and Structures* **17**(4), 045010-1 – 045010-14.
32. Wallmersperger T, Akle BJ, Leo DJ, Kröplin B. 2008 Electrochemical response in ionic polymer transducers: An experimental and theoretical study. *Composites Science and Technology* **68**(5), 1173 – 1180.
33. Ehrenhofer A, Elstner M, Wallmersperger T. 2018 Normalization of hydrogel swelling behavior for sensoric and actuatoric applications. *Sensors and Actuators B: Chemical* **255**(2), 1343 – 1353.
34. Xin F, Lu TJ. 2018 Acousto-thermo-mechanical deformation of hydrogels coupled with chemical diffusion. *Proceedings of the Royal Society A: Mathematical, Physical and Engineering Sciences* **474**(2217), 20180293-1 – 20180293-17.
35. Gebhart P, Wallmersperger T. 2019 A general framework for the modeling of porous ferrogels at finite strains. *Journal of the Mechanics and Physics of Solids* **122**, 69 – 83.
36. Rossi M, Wallmersperger T, Neukamm S, Padberg-Gehle K. 2017 Modeling and Numerical Simulation of Electrochemical Cells under Applied Voltage. *Electrochimica Acta* **258**, 241 –254.
37. Rossi M, Wallmersperger T. 2018 Thermodynamically consistent three-dimensional electrochemical model for polymeric membranes. *Electrochimica Acta* **283**, 1323 – 1338.
38. Pritchard RH, Terentjev EM. 2013 Swelling and de-swelling of gels under external elastic deformation. *Polymer* **54**, 6954–6960.
39. Mishima R, Nakao A, Sakurai S, Urayama K. 2017 Peculiar extensibility of swollen statistical hydrogels with structural nanoheterogeneities. *Polymer* **115**, 28–36.
40. Fujine M, Takigawa T, Urayama K. 2015 Strain-Driven Swelling and Accompanying Stress Reduction in Polymer Gels under Biaxial Stretching. *Macromolecules* **48**, 3622–3628.